Giant magnetoresistance in semiconductor/granular film heterostructures with cobalt nanoparticles

L. V. Lutsev,[1,*] A. I. Stognij,[2] and N. N. Novitskii[2]
[1]*A.F. Ioffe Physico-Technical Institute, Russian Academy of Sciences, 194021 St. Petersburg, Russia*
[2]*Scientific-Practical Materials Research Center, National Academy of Sciences of Belarus, 220072 Minsk, Belarus*
(Received 27 May 2009; revised manuscript received 16 October 2009; published 23 November 2009)

We have studied the electron transport in SiO_2(Co)/GaAs and SiO_2(Co)/Si heterostructures, where the SiO_2(Co) structure is the granular SiO_2 film with Co nanoparticles. In SiO_2(Co)/GaAs heterostructures giant magnetoresistance effect is observed. The effect has positive values, is expressed when electrons are injected from the granular film into the GaAs semiconductor, and has the temperature-peak-type character. The temperature location of the effect depends on the Co concentration and can be shifted by the applied electrical field. For the SiO_2(Co)/GaAs heterostructure with 71 at. % Co the magnetoresistance reaches 1000 (10^5%) at room temperature. On the contrary, for SiO_2(Co)/Si heterostructures magnetoresistance values are very small (4%) and for SiO_2(Co) films the magnetoresistance has an opposite value. High values of the magnetoresistance effect in SiO_2(Co)/GaAs heterostructures have been explained by magnetic field-controlled process of impact ionization. The spin-dependent potential barrier is formed in the accumulation electron layer in the semiconductor near the interface. The impact ionization induced by injected electrons produces holes, which move, are accumulated in the region of the potential barrier and lower the barrier height. The height decrease grows the electron current flowing through the barrier and leads to the enhancement of the avalanche. Due to the formed positive feedback small variations in the barrier height lead to great changes in the current. The applied magnetic field increases the height and reduces the transparency of the barrier. As a result, small feedback reduction suppresses the onset of the impact ionization. The spin-dependent potential barrier is formed by the exchange interaction between electrons in the accumulation electron layer in the semiconductor and *d* electrons of Co. Existence of spin-polarized localized electron states in the accumulation layer results in the temperature-peak-type character of the barrier, which is manifested in the magnetoresistance effect. Spin injectors and efficient magnetic sensors on the base of ferromagnet/semiconductor heterostructures with holes traps and quantum wells containing spin-polarized localized electrons in the semiconductor at the interface are considered.

DOI: 10.1103/PhysRevB.80.184423 PACS number(s): 75.47.De, 72.25.Dc

I. INTRODUCTION

Electron spin transport in ferromagnet/semiconductor (FM/SC) heterostructures has recently become an active area of research. The manipulation of carrier spin in FM/SC heterostructures offers enhanced functionality of spin-electronic devices such as spin transistors, sensors, and magnetic memory cells.[1,2] FM/SC heterostructures are intended to employ as magnetoresistance cells and injectors of spin-polarized electrons in SCs.[3–5] For practical applications it is highly desirable to realize these effects at room temperature. Spin transport phenomena and magnetoresistance are observed on a number of heterostructures.

(1) Spin injection into a nonmagnetic SC is observed at low temperatures in magnetic SC/nonmagnetic SC heterostructures[6–8] and in ferromagnetic metal/nonmagnetic SC.[9–14] At room temperature the spin injection reveals low efficiency.

(2) Spin injection in the ferromagnetic metal/insulator/SC heterostructure is more efficient in comparison with the spin injection from ferromagnetic metal/SC heterostructures.[15–19] The maximum of the spin polarization of injected electrons is achieved for a MgO barrier on GaAs (47% at 290 K).[17]

(3) The giant magnetoresistance (GMR) is observed in metal magnetic multilayers.[20–23] For three-layer structures, the typical values of GMR at room temperature lie in the range 5–8 %.

(4) High values of tunneling magnetoresistance (TMR) are realized on the base of magnetic tunnel junction (MTJ) structures.[17,24–33] Spin-dependent tunneling is not only determined by the properties of ferromagnetic electrodes but also depends on the electronic structure of insulator barriers. The maximum TMR ratio of 500% at room temperature was observed in the MTJ structure with the MgO barrier.[33]

(5) Extremely large magnetoresistance can be achieved by use magnetic field-dependent avalanche breakdown phenomena.[34–42] Values of the magnetoresistance effect based on the avalanche breakdown reach 10^5% in the Au/semi-insulating GaAs Schottky diode at room temperature.[36]

Although important results in the spin injection and in the magnetoresistance have been obtained, the efficient spin injection at room temperature has not been achieved. Besides, for some applications it is necessary to use sensors with high magnetoresistance values. These problems can be resolved by using FM/SC heterostructures with spin-dependent potential barrier, which governs the kinetic energy of injected electrons and the onset of impact ionization.[37–39] In these heterostructures FM is a granular film with *d* (or *f*) metal nanoparticles. In contrast with metal/SC structures with the Schottky barrier based on the magnetic field-dependent avalanche breakdown phenomena,[36,40–42] the transparency of the spin-dependent potential barrier, which is formed in the spin-polarized accumulation electron layer in the SC near the in-

terface, is characterized by the temperature-peak dependence and is differ for different spin orientations of injected electrons. The barrier is due to the exchange interaction between $d(f)$ electrons in the FM at the interface and electrons in the SC, which polarizes electrons in the accumulation layer.

In this paper, we study the magnetoresistance in $SiO_2(Co)/GaAs$ and $SiO_2(Co)/Si$ heterostructures, where the $SiO_2(Co)$ is the granular SiO_2 film with Co nanoparticles. Sample preparation and experimental results are presented in Sec. II. The effect is more expressed when electrons are injected from the granular film into the SC, therefore, the magnetoresistance has been called the injection magnetoresistance (IMR).[37,38] For $SiO_2(Co)/GaAs$ heterostructures the IMR value reaches 1000 (10^5%) at room temperature, which is two to three orders higher than maximum values of the GMR in metal magnetic multilayers and the TMR in MTJ structures. On the contrary, for $SiO_2(Co)/Si$ heterostructures the magnetoresistance values are very small and for $SiO_2(Co)$ films the intrinsic magnetoresistance is of a negative value. The IMR effect has a temperature-peak-type character and its temperature location can be shifted by the applied electrical field. High values of the IMR effect in $SiO_2(Co)/GaAs$ heterostructures and the temperature-peak-type character are explained in Sec. III by the theoretical model of a magnetic field-controlled avalanche process provided by electrons passed through the spin-dependent potential barrier in the accumulation layer at the interface.[39] In Sec. IV we consider FM/SC heterostructures with holes traps and quantum wells containing spin-polarized localized electrons in the SC at the interface as efficient room-temperature spin injectors and magnetic sensors. These heterostructures can be used as bioanalytical sensors with higher sensitivity in comparison with GMR sensors[43,44] and as injectors in spin-valve transistors and in spin field-effect transistor structures.[45–47]

II. EXPERIMENTAL RESULTS

A. Sample preparation

Experiments were performed on samples of amorphous silicon dioxide films containing cobalt nanoparticles grown (1) on gallium arsenide, $(SiO_2)_{100-x}Co_x/GaAs$ [or shorter $SiO_2(Co)/GaAs$], (2) on silicon, $(SiO_2)_{100-x}Co_x/Si$ [or shorter $SiO_2(Co)/Si$], and (3) on quartz substrates. n-GaAs substrates with thickness of 0.4 mm are of the (100)-orientation type. Electrical resistivity of GaAs chips was measured by the dc four-probe method at room temperature and was equal to 0.93×10^5 Ω cm. The 0.4 mm n-Si substrates have the orientation of (100) and the resistivity of 3.7 Ω cm. Prior to the deposition process, substrates were polished by a low-energy oxygen ion beam.[48,49] The roughness height of the polished surfaces did not exceed 0.5 nm.

The $SiO_2(Co)$ films were deposited by ion-beam cosputtering of the composite cobalt-quartz target onto GaAs, Si, and quartz substrates heated to 200 °C. The concentration of Co nanoparticles in the silicon dioxide deposit was varied by changing the ratio of cobalt and quartz target areas. The film composition was determined by the nuclear physical methods of element analysis using a deuteron beam of the electrostatic accelerator (PNPI, Gatchina, Leningrad region, Russia). The cobalt to silicon atomic ratio was measured by the Rutherford backscattering spectrometry of deuterons. The oxygen concentration in films was determined by the method of nuclear reaction with deuterons at $E_d=0.9$ MeV: $^{16}O+d\rightarrow p+^{17}O$. This technique is described in more detail elsewhere.[50] For the samples studied, the relative content of cobalt x and the film thickness are listed in Table I. The average size of Co particles was determined by the small-angle x-ray scattering and increased as the concentration of x grows: from 2.7 nm at $x=38$ at. % to 4.4 nm at $x=82$ at. %. Cobalt particles are in the ferromagnetic state.[51–53] The samples with high concentration of Co (71 and 82 at. %) exhibit ferromagnetic behavior confirmed by the presence of a domain structure (Fig. 1) obtained with high vacuum magnetic field microscope HV-MFM SOLVER (NT-MDT Co). The period of the domain structure for the $SiO_2(Co)/GaAs$ sample with 82 at. % Co is equal to 3.9 μm, which is smaller than the domain period for the same $SiO_2(Co)$ film on the Si substrate (6.0 μm). The samples with low concentration of Co are superparamagnetic.

TABLE I. Properties of $SiO_2(Co)$ films sputtered on Ga As, Si, and quartz substrates.

Co concentration x (at. %)	Film thickness (nm)		
	GaAs substrate	Si substrate	Quartz substrate
38	86	86	860
45	81	81	810
54	90	90	900
71	95	95	950
82	95	95	950

Electrical resistivity of $SiO_2(Co)$ films was measured by the dc four-probe method on $SiO_2(Co)$/quartz heterostructures at room temperature. As the Co content increased, the resistivity of $SiO_2(Co)$ films decreased from 1.46×10^2 Ω cm (38 at. %) to 1.1 Ω cm (82 at. %).

B. Experiment

We have studied the electron transport and magnetoresistance in $SiO_2(Co)/SC$ heterostructures (Table I). One contact was on the semiconductor substrate and the other on the $SiO_2(Co)$ granular film. All $SiO_2(Co)/GaAs$ samples and $SiO_2(Co)/Si$ samples with the Co concentration, which is equal to or lesser than 71 at. %, have current-voltage dependencies of the diode type. At positive voltages for structures of the diode type of the current-voltage characteristic electrons are injected from the granular film into the SC and the current density j is high. For the applied voltage $U=90$ V the current density reaches 6.0×10^{-2} A/cm^2. When the applied voltage U is negative, electrons drift from the SC into the granular film and the current density is low. For $SiO_2(Co)/Si$ heterostructure with high Co content (82 at. %), the current-voltage characteristic is close to the

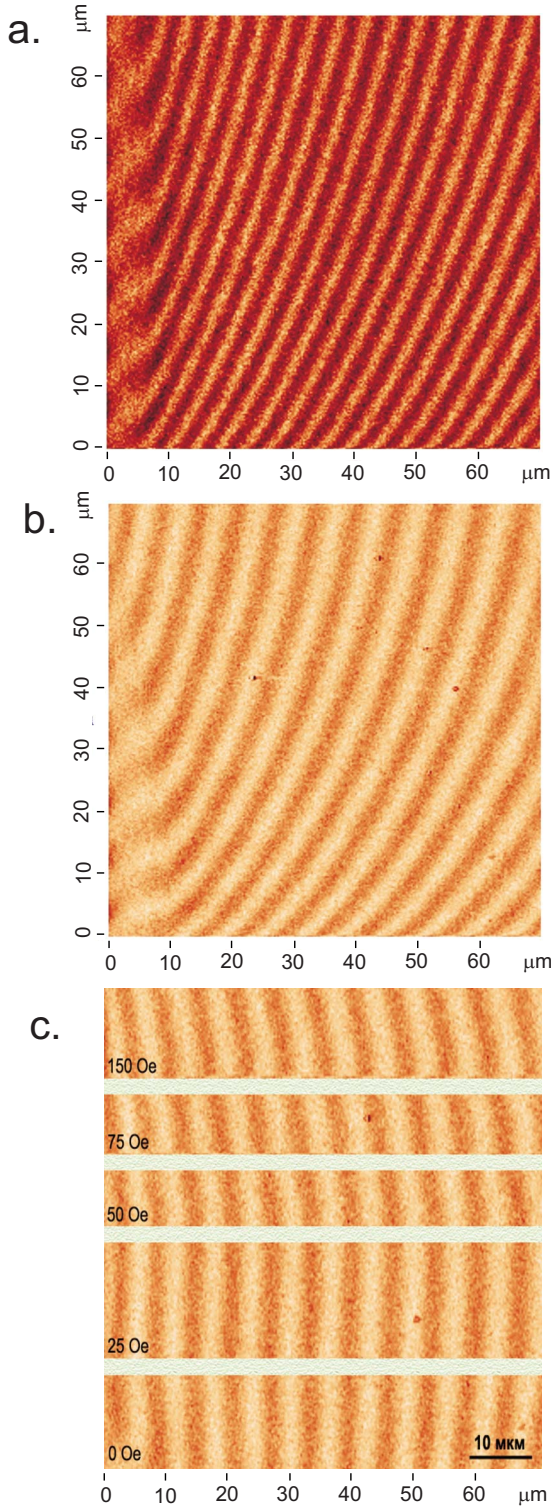

FIG. 1. (Color online) Magnetic field microscope image of the domain structure on samples with SiO_2(Co) films with 82 at. % Co (a) on the GaAs substrate and (b) on the Si substrate. (c) Influence of the applied magnetic field on the domain structure on the SiO_2(Co)/Si sample with 82 at. % Co.

dependence of the Ohm type. Figure 2 shows temperature dependencies of the electron inject current density j for the SiO_2(Co)/GaAs structure with the Co concentration x =71 at. % at the applied voltage U=70 V. The resistivity of

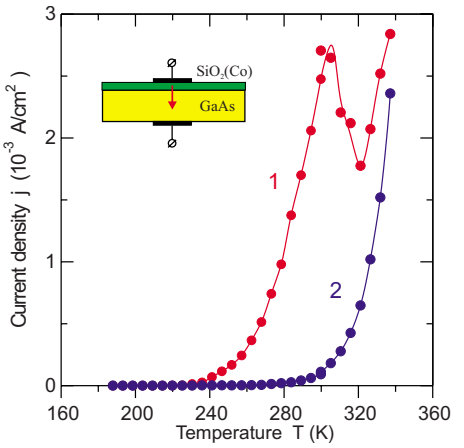

FIG. 2. (Color online) Temperature dependencies of the inject current j for the SiO_2(Co)/GaAs structure with the Co concentration 71 at. % at the applied voltage U=70 V. (1) In the absence of a magnetic field and (2) in the magnetic field H=10 kOe. H is parallel to the surface of the SiO_2(Co) film. Solid lines are guides for the eye.

GaAs is higher than the resistivity of the film and the applied voltage primarily falls on the SC substrate. We notice that at the temperature T=320 K in the absence of a magnetic field the inject current has local minimum. The electron inject current flowing from the granular film into the SC is suppressed by the magnetic field. The magnetic field H is equal to 10 kOe and is parallel to the surface plane of the granular film. At $T>320$ K temperature dependencies of the inject current in the absence of a magnetic field and in the field H are close.

Figure 3 illustrates the effect of the magnetic field on the current-voltage characteristic in the case of the electron injection into the SC for the SiO_2(Co)/GaAs structure with 71 at. % Co. For $U>52$ V, a sharp increase in current due to the process of impact ionization is observed. The applied magnetic field postpones this process to higher electric fields. The magnetic field H is parallel to the film surface. If the magnetic field is perpendicular to the film surface, the depen-

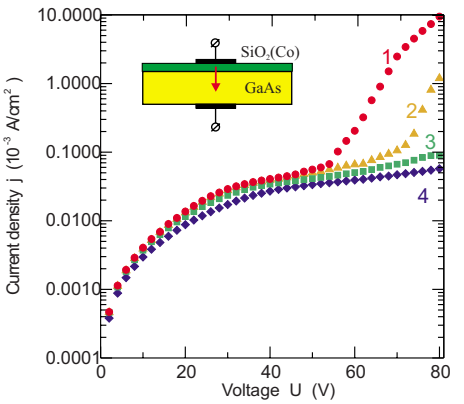

FIG. 3. (Color online) Current-voltage characteristic for the electron injection into the semiconductor for the SiO_2(Co)/GaAs structure with 71 at. % Co at different magnetic fields: (1) H=0, (2) 5 kOe, (3) 10 kOe, and (4) 15 kOe. H is parallel to the surface of the SiO_2(Co) film.

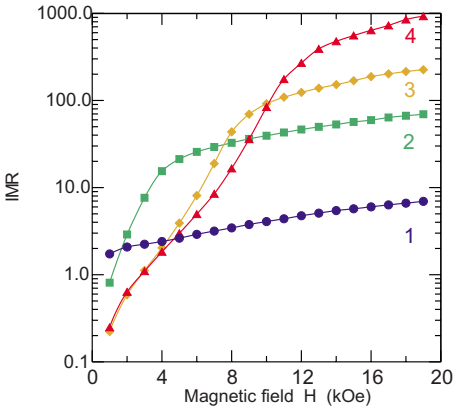

FIG. 4. (Color online) Injection magnetoresistance ratio versus the magnetic field H at room temperature for the SiO_2(Co)/GaAs structure with 71 at. % Co at applied voltages: (1) $U=60$ V, (2) 70 V, (3) 80 V, and (4) 90 V. H is parallel to the surface of the SiO_2(Co) film. Solid lines serve to guide the eye.

dence of the current on the magnetic field H is weaker because of the demagnetization factor of the film but the magnetic suppression of the current is still observed.

By analogy with GMR and TMR coefficients,[17,20–33] we define the injection magnetoresistance coefficient IMR as the ratio[37–39]

$$\mathrm{IMR} = \frac{R(H) - R(0)}{R(0)} = \frac{j(0) - j(H)}{j(H)}, \qquad (1)$$

where $R(0)$ and $R(H)$ are the resistances of the SiO_2(Co)/SC heterostructure without a field and in the magnetic field H, respectively; $j(0)$ and $j(H)$ are the current densities flowing in the heterostructure in the absence of a magnetic field and in the field H. The IMR ratio for the SiO_2(Co)/GaAs structure with 71 at. % Co at different applied voltages at room temperature (21 °C) is shown in Fig. 4 as a function of the magnetic field H parallel to the film. As seen from Fig. 4, the IMR coefficient increases with the growth of the applied voltage. At the voltage $U=90$ V for this structure the value of IMR reaches up to 1000 (10^5%) at room temperature at the field $H=19$ kOe. This is two to three orders higher than maximum values of GMR in metal magnetic multilayers and TMR in MTJ structures.

The IMR ratio for SiO_2(Co)/GaAs structures versus the Co concentration x in the in-plane field $H=20$ kOe at the applied voltage $U=60$ V for different current directions is presented in Fig. 5. The IMR coefficient has maximum values for structures with Co concentrations in the range (54–71 at. %), when electrons are injected from the SiO_2(Co) film into the SC. The IMR ratio decreases for structures with higher ($x>71$ at. %) and lower ($x<54$ at. %) Co concentrations. On the contrary, in the case of the opposite current direction (electrons drift from the SC into the granular film) the magnetoresistance effect becomes less expressed.

As we can see from Figs. 4 and 5, for SiO_2(Co)/GaAs structures the IMR coefficient can reach high values at room temperature. In contrast with this, for SiO_2(Co)/Si structures

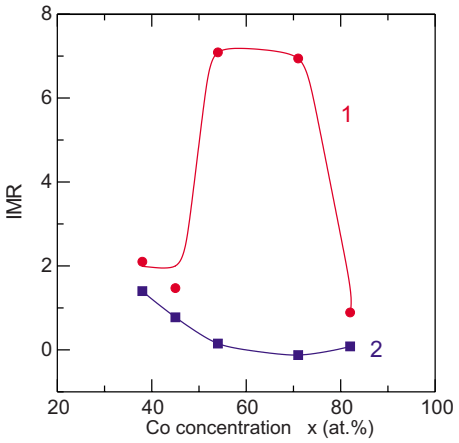

FIG. 5. (Color online) Magnetoresistance ratio versus the Co concentration x for SiO_2(Co)/GaAs structures in the field $H=20$ kOe at the applied voltage $U=60$ V for different current directions. (1) Electrons are injected from the SiO_2(Co) film into GaAs, (2) electrons drift from GaAs into the granular film. H is parallel to the surface of the SiO_2(Co) film. Solid lines serve to guide the eye.

magnetoresistance values are very small and the intrinsic magnetoresistance of SiO_2(Co) films has negative values (Fig. 6). The magnetoresistance (MR) ratio for SiO_2(Co) films is determined by the relation analogous to Eq. (1). For SiO_2(Co)/Si structures electrons are injected from the granular film into the Si substrate. Taking into account low values of the resistivity of Si substrates, experiments were carried out at the applied voltage $U=3$ V. For SiO_2(Co) films the intrinsic magnetoresistance ratio was measured by the dc four-probe method on SiO_2(Co)/quartz samples in the current-in-plane geometry at the applied voltage $U=60$ V at room temperature.

Temperature dependencies of the magnetoresistance can give useful information about the nature of the magnetoresistance effect. Figure 7 presents temperature dependencies of the intrinsic magnetoresistance for SiO_2(Co) films with low ($x=38$ at. %) and high ($x=71$ at. %) Co concentrations and for the SiO_2(Co,71 at. %)/Si structure. Experiments

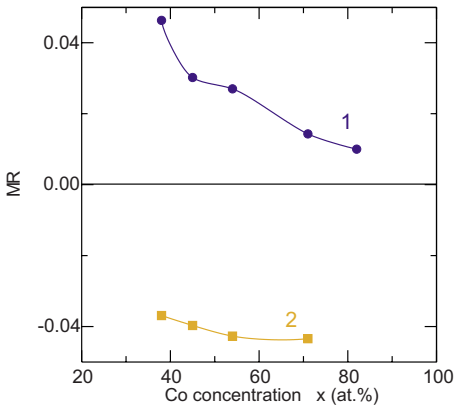

FIG. 6. (Color online) Magnetoresistance ratio versus the Co concentration x for (1) SiO_2(Co)/Si structures and for (2) SiO_2(Co) films in the in-plane magnetic field $H=20$ kOe. Solid lines serve to guide the eye.

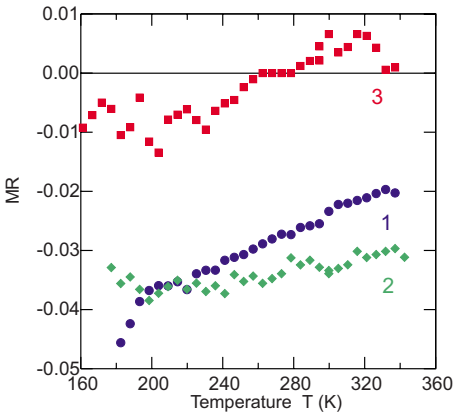

FIG. 7. (Color online) Temperature dependencies of the magnetoresistance for SiO_2(Co) films (1) with x=38 at. % Co, (2) with x=71 at. % Co, and (3) for the SiO_2(Co)/Si structure with x =71 at. % Co content in the in-plane magnetic field H=10 kOe.

were carried out at the applied voltage U=60 V for SiO_2(Co) films and at U=3 V for the SiO_2(Co)/Si structure. The magnetic field H=10 kOe is parallel to the surface of the granular film. It can be seen that temperature decreasing causes to the growth of the absolute value of the intrinsic magnetoresistance for SiO_2(Co) films. For the SiO_2(Co)/Si structure electrons are injected from the granular film into the semiconductor and temperature decreasing leads to the change in the magnetoresistance sign.

Temperature dependencies of the IMR for SiO_2(Co)/GaAs structures essentially differ from the above-mentioned dependencies for SiO_2(Co)/Si structures and SiO_2(Co) films. They have a peak-type character (Figs. 8 and 9). The temperature location of the peak depends on the Co concentration and can be shifted by the applied electrical field. Figure 8 shows temperature dependencies of the IMR for SiO_2(Co)/GaAs with 71 at. % Co at different applied voltages, when electrons are injected from the granular film into the GaAs substrate. Increasing voltage U causes to a

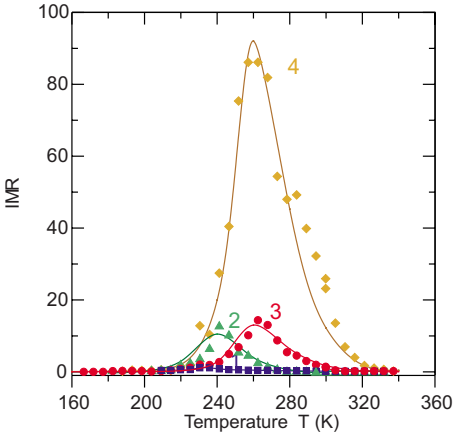

FIG. 8. (Color online) Temperature dependencies of the injection magnetoresistance for the SiO_2(Co)/GaAs structure with x =71 at. % Co content in the in-plane magnetic field H=10 kOe at applied voltages: (1) U=40 V, (2) 50 V, (3) 60 V, and (4) 70 V. Solid lines are theoretical fittings.

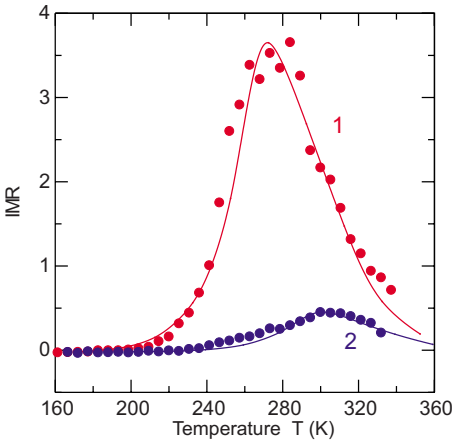

FIG. 9. (Color online) Temperature dependencies of the magnetoresistance for the SiO_2(Co)/GaAs structure with x=38 at. % Co content in the in-plane magnetic field H=10 kOe at the applied voltage U=60 V. (1) Electrons are injected from the SiO_2(Co) film into GaAs, (2) electrons drift from GaAs into the granular film. Solid lines are theoretical fittings.

shift of the peak to higher temperatures. At the same time, the voltage growth leads to an increase in the peak magnitude. For SiO_2(Co)/GaAs structure with lower Co content (x=38 at. %, Fig. 9), the temperature peak of the IMR has higher value of width. For the case, when electrons move from GaAs into the SiO_2(Co) film, the IMR peak is located at higher temperature and its magnitude is lower.

III. THEORETICAL MODEL AND EXPLANATION OF EXPERIMENTAL RESULTS

A. Theoretical model

Explanation of the IMR effect is based on the theoretical model of the magnetic field-controlled avalanche process triggered by electrons passed through the spin-dependent potential barrier in the accumulation layer in the SC at the interface. The impact ionization induced by electrons produces holes, which move and are accumulated in the region of the potential barrier. Existence of holes in this region lowers the barrier height. This leads to the growth of the electron current flowing through the barrier. The electron current growth results in increasing hole concentration in the barrier region and so on. Due to the formed positive feedback small variations in the height of the potential barrier lead to great changes in the flowing current. The electron current growth is accompanied by the appearance of a layer with strong electrical field in the vicinity of the barrier. The change in the electrical field decreases the value of the threshold of the avalanche process making this process easier in the strong-field layer. The applied magnetic field reduces the transparency of the spin-dependent potential barrier. This decreases the kinetic energy of injected electrons, suppresses the impact ionization onset, and reduces the hole concentration. Let us consider formation of the accumulation electron layer in the SC at the interface, the spin-dependent potential barrier, the electrical field distribution, the avalanche process, and the IMR effect caused by the barrier.[39]

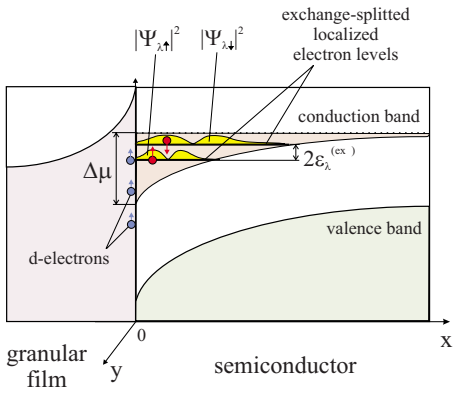

FIG. 10. (Color online) Electronic energy-band structure at the contact region of the ferromagnet/semiconductor.

1. Hamiltonian

In the FM/SC heterostructure the difference of chemical potentials $\Delta\mu$ between the FM and the SC determines bending of the SC conduction band (Fig. 10). We suppose that $\Delta\mu > 0$ and there is formed an accumulation electron layer in the SC. d electrons in the FM at the interface and electrons in the accumulation electron layer in the SC are coupled by the exchange interaction $J_0(\vec{r}-\vec{R})$. The Hamiltonian of the model is written in the form

$$\mathcal{H} = \mathcal{H}_e + \mathcal{H}_{ed} + \mathcal{H}_\varphi + \mathcal{H}_s,$$

where

$$\mathcal{H}_e = \sum_\alpha \int \Psi_\alpha^+(\vec{r})\left[-\frac{\hbar^2}{2m}\Delta - \mu - e\varphi(\vec{r})\right]\Psi_\alpha(\vec{r})d\vec{r}$$

is the Hamiltonian of electrons with the mass m and the charge e in the SC in the electrical field with the potential $\varphi(\vec{r})$. μ is the chemical potential. $\Psi_\alpha^+(\vec{r}) = \Sigma_\lambda \psi_\lambda^*(\vec{r}) a_{\lambda\alpha}^+$ and $\Psi_\alpha(\vec{r}) = \Sigma_\lambda \psi_\lambda(\vec{r}) a_{\lambda\alpha}$ are the second-quantized wave functions of an electron with a spin $\alpha = \uparrow, \downarrow$. $a_{\lambda\alpha}^+$ and $a_{\lambda\alpha}$ are the creation and annihilation Fermi operators, respectively, for an electron with the wave function $\psi_\lambda(\vec{r})$ with the multi-index λ.

$$\mathcal{H}_{ed} = -\sum_{\vec{R}} \int J_0(\vec{r}-\vec{R})(\vec{S}(\vec{R}), \vec{\sigma}(\vec{r}))d\vec{r}$$

is the exchange interaction Hamiltonian between the spin density $\vec{\sigma}(\vec{r})$ of electrons in the SC and spins $\vec{S}(\vec{R})$ of d electrons in the FM. The vector spin-density operator $\vec{\sigma}(\vec{r})$ is determined by operators $\Psi_\alpha(\vec{r})$ and $\Psi_\alpha^+(\vec{r})$

$$\sigma_x(\vec{r}) = \Psi_\uparrow^+(\vec{r})\Psi_\downarrow(\vec{r}) + \Psi_\downarrow^+(\vec{r})\Psi_\uparrow(\vec{r}),$$

$$\sigma_y(\vec{r}) = -i\Psi_\uparrow^+(\vec{r})\Psi_\downarrow(\vec{r}) + i\Psi_\downarrow^+(\vec{r})\Psi_\uparrow(\vec{r}),$$

$$\sigma_z(\vec{r}) = \Psi_\uparrow^+(\vec{r})\Psi_\uparrow(\vec{r}) - \Psi_\downarrow^+(\vec{r})\Psi_\downarrow(\vec{r}).$$

The Hamiltonian

$$\mathcal{H}_\varphi = -\frac{1}{8\pi}\int [\nabla\varphi(\vec{r})]^2 d\vec{r}$$

describes the classical inner electrostatic field $\varphi(\vec{r})$.

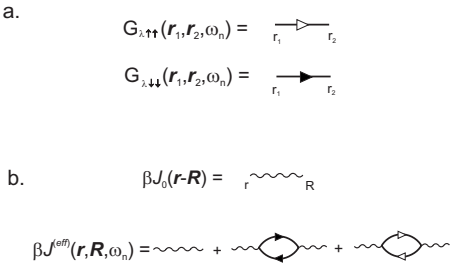

FIG. 11. (a) Temperature electron Green's functions with the spin ↑ and ↓. (b) Bare and effective exchange interactions.

$\mathcal{H}_s$ is the Hamiltonian described the interaction between spins $\vec{\sigma}(\vec{r})$ and $\vec{S}(\vec{r})$, and the magnetic field $\vec{H}$

$$\mathcal{H}_s = -g\mu_B \sum_{\vec{R}} (\vec{H}, \vec{S}(\vec{r})) - g\mu_B \int (\vec{H}, \vec{\sigma}(\vec{r}))d\vec{r},$$

where g and μ_B are the Landé factor and the Bohr magneton, respectively.

In order to find the effective exchange interaction between spins $\vec{S}(\vec{R})$ of d electrons in the FM and the spin $\vec{\sigma}^{(in)}(\vec{r})$ of an injected electron with the wave function $\psi_\alpha^{(in)}(\vec{r})(\alpha = \uparrow, \downarrow)$ and the spin-dependent potential barrier, the temperature diagram technique is used.[54,55] Before this we consider formation of the accumulation electron layer.

2. Formation of the accumulation electron layer

In the self-consistent-field approximation of the diagram expansion electrons of the conduction band in the SC and the inner self-consistent electrical field are described by the following equations.

(1) Equation for the electron wave function in the SC

$$\left[-\frac{\hbar^2}{2m}\frac{d^2}{dx^2} - e\varphi(x)\right]\chi_\nu(x) = \varepsilon_\nu^{(0)}\chi_\nu(x), \tag{2}$$

where $\psi_\lambda(\vec{r}) = V^{-1/2}\chi_\nu(x)\exp(iq_y y + iq_z z)$ is the electron wave function in the volume V of the SC with the multi-index $\lambda = (\nu, q_y, q_z)$ and the energy spectrum $\varepsilon_\lambda = \varepsilon_\nu^{(0)} + \hbar^2(q_y^2 + q_s^2)/2m$.

(2) Equation for the inner self-consistent electrical field

$$\Delta\varphi(\vec{r}) = 4\pi e\left\{\sum_{\lambda,\omega_n}[G_{\lambda\uparrow\uparrow}(\vec{r},\vec{r},\omega_n) + G_{\lambda\downarrow\downarrow}(\vec{r},\vec{r},\omega_n) - G_{\lambda\uparrow\uparrow}^{(0)}(\vec{r},\vec{r},\omega_n) - G_{\lambda\downarrow\downarrow}^{(0)}(\vec{r},\vec{r},\omega_n)]\right\}, \tag{3}$$

where

$$G_{\lambda\alpha_1\alpha_2}(\vec{r}_1,\vec{r}_2,\omega_n) = \frac{\psi_\lambda^*(\vec{r}_1)\psi_\lambda(\vec{r}_2)\delta_{\alpha_1\alpha_2}}{\beta(i\hbar\omega_n - E_{\lambda\alpha_1} + \mu)} \tag{4}$$

are electron Green's functions [Fig. 11(a)], $\beta = 1/kT$, k is the Boltzmann constant, T is the temperature, $\hbar\omega_n = (2n+1)\pi/\beta$, n is an integer,

$$E_{\lambda\alpha} = \varepsilon_\lambda \mp \varepsilon_\lambda^{(\mathrm{ex})}. \tag{5}$$

The upper sign in Eq. (5) corresponds to $\alpha = \uparrow$; the lower sign, to $\alpha = \downarrow$. The energy $\varepsilon_\lambda^{(\mathrm{ex})}$ is determined by the exchange

Hamiltonian $\mathcal{H}_{ed}$ in the self-consistent-field approximation

$$\varepsilon_{\lambda}^{(\mathrm{ex})} = -\sum_{\vec{R}} \int J_0(\vec{r}-\vec{R})(\langle \vec{S}(\vec{R})\rangle_0, \langle \vec{\sigma}(\vec{r})\rangle_0) d\vec{r}. \tag{6}$$

$\langle \vec{S}(\vec{R})\rangle_0$ and $\langle \vec{\sigma}(\vec{r})\rangle_0$ are the statistical-average d-electron spin in the FM and the electron-spin density in the SC, respectively. $G^{(0)}_{\lambda\alpha\alpha}$ are electron Green's functions determined in the single SC in the absence of the electrical field.

(3) To the above-mentioned equations it is necessary to add relationship between the chemical potential μ and the electron concentration n_0 in the single SC

$$n_0 = \frac{8\pi e}{V} \sum_{\vec{q}=(q_x,q_y,q_z)} n_F[\beta(\hbar^2|\vec{q}|^2/2m - \mu)], \tag{7}$$

where $n_F(a)=[\exp(a)+1]^{-1}$.

Equations (2), (3), and (7) are simultaneous equations in unknowns: the wave function $\chi_\nu(x)$, the energy $\varepsilon^{(0)}_\nu$, the electrical potential $\varphi(x)$, and the chemical potential μ in the SC. Taking into account that at the interface of the heterostructure ($x=0$) the potential $\varphi(x)$ is determined by the difference of chemical potentials $\Delta\mu$ between the SC and the FM, $\varphi(0)=\Delta\mu/e$, and at a great distance from the interface, when $x\to\infty$, the potential $\varphi(x)$ tends to zero, we numerically can solve Eqs. (2), (3), and (7).

3. Effective exchange interaction and the spin-dependent potential barrier

The effective exchange interaction and the spin-dependent potential barrier for injected electrons are found in the next approximation of the diagram expansion. This is the one-loop approximation with respect to the bare exchange interaction $J_0(\vec{r}-\vec{R})$ [Fig. 11(b)]. In this approximation we take into account solutions of Eqs. (2), (3), and (7) made in the self-consistent-field approximation and find the effective exchange interaction

$$J^{(\mathrm{eff})}(\vec{r},\vec{R},\omega_n) = J_0(\vec{r}-\vec{R}) + J_1(\vec{r},\vec{R},\omega_n),$$

where the interaction J_1 has the form

$$\begin{aligned} J_1(\vec{r},\vec{R},\omega_n) = -\beta \int\int J_0(\vec{r}-\vec{r}_1) \\ \times \sum_{k,\lambda_1,\lambda_2} [G_{\lambda_1\uparrow\uparrow}(\vec{r}_1,\vec{r}_2,\omega_k) G_{\lambda_2\uparrow\uparrow}(\vec{r}_1,\vec{r}_2,\omega_k+\omega_n) \\ + G_{\lambda_1\downarrow\downarrow}(\vec{r}_1,\vec{r}_2,\omega_k) G_{\lambda_2\downarrow\downarrow}(\vec{r}_1,\vec{r}_2,\omega_k+\omega_n)] \\ \times J_0(\vec{r}_2-\vec{R}) d\vec{r}_1 d\vec{r}_2. \end{aligned} \tag{8}$$

In the relation (8) the Green's functions $G_{\lambda\alpha_1\alpha_2}$ [Eq. (4)] are expressed via wave functions $\psi_\lambda(\vec{r})$, the chemical potential μ and the electron energy $E_{\lambda\alpha}$ [Eq. (5)]. The interaction J_1 is of the Ruderman, Kittel, Kasuya, and Yosida[56–58] type. Spins of electrons in the accumulation layer shield spins of d electrons in the FM at the interface. As the result of this shielding, the short-range exchange interaction $J_0(\vec{r}-\vec{R})$ is transformed into the long-range effective exchange interaction $J^{(\mathrm{eff})}(\vec{r},\vec{R},\omega_n)$, which changes its sign at a some distance from the interface (Fig. 12). To find the numerical solution, we assume that $J_0(\vec{r}-\vec{R})=J_0\exp(-\xi|\vec{r}-\vec{R}|)$ in Eqs. (6) and (8), where ξ is the reciprocal radius of the exchange interaction and J_0 is determined by the Coulomb interaction with d electrons on a FM atom.[59] Calculations have been drawn, when $\omega_n=0$, $\vec{R}=0$, $\xi=10$ nm^{-1}, $J_0=2$ eV, $|\langle \vec{S}(\vec{R})\rangle_0|=1/2$, $|\langle \vec{\sigma}(\vec{r})\rangle_0|=1/2|\psi_\lambda(\vec{r})|^2$, $\Delta\mu=150$ meV, and $n_0=1\times10^{15}$ cm^{-3} at $T=300$ K for the cubical crystal FM lattice with the lattice constant $a=0.23$ nm. At the distance r_0 the exchange interaction J_1 has a maximum opposite value. If the accumulation layer (quantum well) contains a great number of electron states, the distance r_0 can be evaluated as the half of the period of the Ruderman-Kittel function, $r_0 \approx \frac{1}{2}(\pi/3n_s)^{1/3}$,[56–58] where n_s is the electron density at the interface.

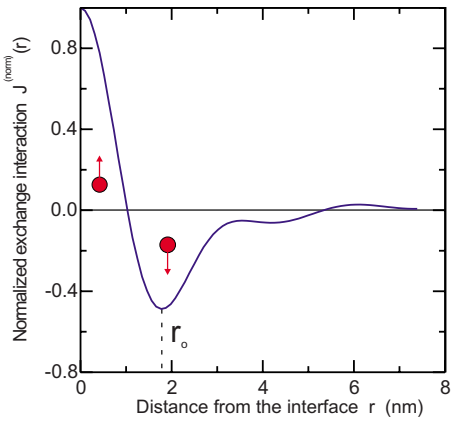

FIG. 12. (Color online) Normalized exchange interaction $J^{(\mathrm{norm})}(r)=J_1(\vec{r},0,0)/J_1(0,0,0)$ for the heterostructure with the difference of chemical potentials $\Delta\mu=150$ meV and with the electron concentration $n_0=1\times10^{15}$ cm^{-3} in the SC at $T=300$ K.

In order to find the spin-dependent potential barrier, we assume that the magnetic field $\vec{H}$ is parallel to the axis Oz. Then, the height of the energy barrier formed by the effective exchange interaction for injected spin-polarized electrons, which move from the interface, is determined by the relation

$$W = \sum_{\vec{R}} \int \langle \sigma_z^{(in)}(\vec{r})\rangle J^{(\mathrm{eff})}(\vec{r},\vec{R},0)\langle S_z(\vec{R})\rangle_0 d\vec{r}, \tag{9}$$

where $\langle \sigma_z^{(in)}(\vec{r})\rangle = \langle \psi_\uparrow^{(in)*}(\vec{r})\psi_\uparrow^{(in)}(\vec{r}) - \psi_\downarrow^{(in)*}(\vec{r})\psi_\downarrow^{(in)}(\vec{r})\rangle$, $\langle S_z(\vec{R})\rangle_0$ is the z projection of the statistical-average d-electron spin at the site $\vec{R}$ at the interface. For calculation of W we assume that the spin density $\langle \sigma_z^{(in)}(\vec{r})\rangle = 1/2\cdot\delta(r-r_0)$. We have found, that, if the accumulation layer contains a small number of localized electron states $\chi_\nu(x)$, which are determined by Eq. (2), then these states give the main contribution to the exchange interaction J_1 in Eq. (8) and to the height of the energy barrier W [Eq. (9)]. The maximum of the barrier is observed, when the accumulation layer has two sublevels of an exchange-splitted localized electron state (Fig. 10). Exchange-splitted localized states have high values of the exchange energy $\varepsilon_\lambda^{(\mathrm{ex})}$ [Eq. (6)] and this causes to high values of the barrier W [Eq. (9)]. If the accumulation layer does not contain localized states, the magnitude of W sharply falls.

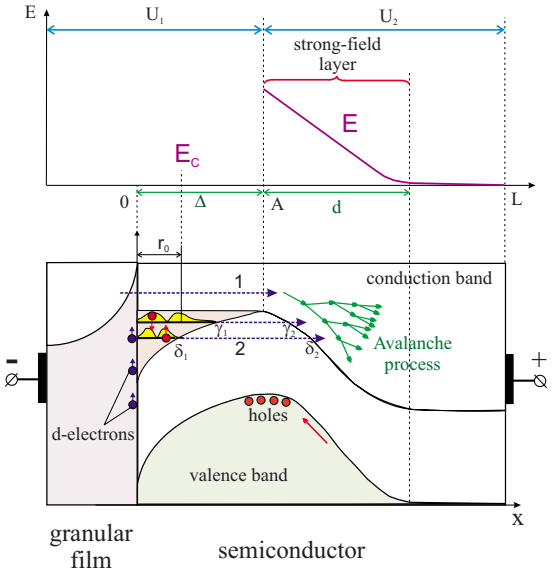

FIG. 13. (Color online) Schematic band diagram at the applied electrical field in the ferromagnet/semiconductor and electrical field distribution in the semiconductor at a high voltage in the avalanche regime. The avalanche process is induced by electrons, which (1) surmount over the spin-dependent potential barrier formed by localized states at the distance r_0 from the interface and (2) tunnel from exchange-splitted localized states.

Dependencies of W on the difference of chemical potentials $\Delta\mu$ and temperature dependencies are presented in Ref. 39.

4. Low voltage. Electrical field distribution below the avalanche threshold

What are changes arisen in the electrical field and in charges in the SC from applied voltage? Let us consider the current beyond the barrier in the range $[A,L]$ (Fig. 13). Theoretical model of the current flowing in this range is analogous to the model of glow discharge.[60,61] We suppose that the process of impact ionization is caused by electrons. Then, current densities of electrons $j_e(x)$ and holes $j_h(x)$ in the SC are given by

$$\frac{dj_e}{dx} = \alpha j_e,$$

$$\frac{dj_h}{dx} = -\alpha j_e, \tag{10}$$

where α is the impact ionization coefficient. The coefficient α has the form[62]

$$\alpha = a_0 \exp\left\{\delta - \left[\delta^2 + \left(\frac{\bar{E}}{E}\right)^2\right]^{1/2}\right\}, \tag{11}$$

where E is the electrical field. For GaAs $a_0 = 0.245 \times 10^6$ cm^{-1}, $\delta = 57.6$, $\bar{E} = 6.65 \times 10^6$ V cm^{-1} and for Si $a_0 = 0.63 \times 10^6$ cm^{-1}, $\delta = 0$, $\bar{E} = 1.23 \times 10^6$ V cm^{-1}. The current j flowing in the SC is the sum of electron and hole currents

$$j = j_e + j_h = e\mu_e nE + e\mu_h pE, \tag{12}$$

where μ_e and μ_h are the mobilities of electrons and holes, respectively; n and p are the electron and hole densities. Holes are arisen during the impact ionization, move to the maximum of the valence band (point A), are accumulated in the region of the point A and disappear by recombination in this region. The existence of holes in the region of the point A decreases the barrier height. This leads to the increase in the electron current j_e flowing through the barrier. Taking this into account and supposing that the hole current at the point L is negligible, we obtain the boundary conditions

$$j_e = \gamma j_h|_A,$$

$$j_h|_L = 0, \quad j_e|_L = j, \tag{13}$$

where γ is the coefficient of the electron current amplification. The electrical field E in the range $[A,L]$ is determined by the difference of hole and electron densities

$$\frac{dE}{dx} = 4\pi e(p - n). \tag{14}$$

Equations (10)–(12) and (14) with the boundary conditions [Eq. (13)] are equations in variables $j_e(x)$, $j_h(x)$, $n(x)$, $p(x)$, and $E(x)$. Solutions of these equations do not express in an analytical form. In order to find solutions, we use step-by-step approximations.

Let us consider the case, when the applied voltage $U = U_1 + U_2$ (Fig. 13) is low and the electrical field $E(x)$ in the range $[A,L]$ is close to a constant value E_0. Then, in the first approximation with respect to $|(E(x) - E_0)/E_0|$, Eq. (10) with the boundary conditions [Eq. (13)] give

$$j_e = j \exp[\alpha(x - L)],$$

$$j_h = j\{1 - \exp[\alpha(x - L)]\}, \tag{15}$$

where α and γ are functional dependent variables expressed by the formula

$$\alpha(L - \Delta) = \ln(1 + 1/\gamma). \tag{16}$$

The relationship [Eq. (16)] describes the balance between the ionization process and incoming (outgoing) holes and electrons in the region of the point A and on the contact L. If $\mu_e \gg \mu_h$ and $\alpha(L - \Delta) \gg 1$, then on the most part of the range $[A,L]$

$$j_h \gg j_e, \quad p = \frac{j}{e\mu_h E}, \quad \frac{n}{p} = \frac{j_e \mu_h}{j_h \mu_e} \ll 1.$$

In this case, Eq. (14) is rewritten in the approximation form

$$\frac{dE}{dx} = 4\pi e p = \frac{4\pi j}{\mu_h E}. \tag{17}$$

Solution of Eq. (17) is

$$E(x) = E_A\left(1 - \frac{x-\Delta}{d}\right)^{1/2}, \tag{18}$$

where E_A is the electrical field at the point A, $d=\mu_h E_A^2/8\pi j$. Solution of Eq. (18) can be used to solve Eq. (10) in the next approximations and to improve solutions in Eq. (15). After this procedure we can find more precise solution of Eq. (14) and so on.

In the first approximation, from solution in Eq. (18) one can see that when $d=L-\Delta$, the electrical field $E(x)$ leads to 0 at $x\to L$. Decreasing E at $x=L$ occurs at the current density

$$j_0 = \frac{\mu_h U_2^2}{8\pi(L-\Delta)^3},$$

where U_2 is the voltage on the SC range $[A,L]$. At the current density j_0 the electrical field distribution is essentially changed. In the vicinity of the barrier a layer of thickness d with strong electrical field appears.

5. High voltage. Current-voltage characteristics at the avalanche process

Let us solve Eqs. (10)–(12) and (14) in the first approximation at high voltage, when the layer with strong electrical field with the thickness d is formed (Fig. 13). We suppose that the electrical field in this layer is much greater than the electrical field at $x>\Delta+d$. Then, for the strong-field layer the relation [Eq. (16)] of the balance between the ionization process and incoming (outgoing) holes and electrons can be rewritten in the form

$$\int_{\Delta}^{d+\Delta} \alpha[E(x)]dx = \ln(1+1/\gamma). \tag{19}$$

The voltage U_2 drops on the strong-field layer

$$U_2 = \int_{\Delta}^{d+\Delta} E(x)dx. \tag{20}$$

Taking into account Eq. (11) and using the average value E_d of the field $E(x)$ in the strong-field layer, from Eqs. (19) and (20) we get

$$E_d = \bar{E}\{[\delta + \ln(a_0 d) + C]^2 - \delta^2\}^{-1/2},$$

$$U_2 = E_d d, \tag{21}$$

where $C=-\ln\ln(1+1/\gamma)$. In order to find the current density j, we consider the vicinity of the point A. From Eq. (17) one can find that

$$p = (4\pi e)^{-1}\frac{dE}{dx} = \frac{E_d}{4\pi e d}.$$

Taking this and Eq. (12) into account, we get

$$j = j_e + j_h = (1+\gamma)ep\mu_h E_d = \frac{(1+\gamma)\mu_h E_d^2}{4\pi d}. \tag{22}$$

Relations (21) and (22) determine the current-voltage characteristic. The thickness d of the strong-field layer is the parameter. The current-voltage characteristic has a minimum and descending and ascending branches. When the current $j>j_0=\mu_h U_2^2/8\pi(L-\Delta)^3$, the current and the electrical field distribution are unstable. The stable equilibrium is achieved in the minimum of the voltage U_2 with respect to d

$$\frac{\partial U_2}{\partial d} = 0.$$

The minimum value of U_2 is reached at the thickness

$$d_m = a_0^{-1}\ln(1+1/\gamma)\exp[(1/2+\delta^2)^{1/2} + 1/2 - \delta]. \tag{23}$$

It is needed to note that the developed theoretical model of the avalanche process is analogous to the model of glow discharge.[60,61] The potential drops rapidly in the strong-field layer with thickness d close to the barrier. The fact that in SCs voltage drops are concentrated mainly in vicinities of contacts (strong-field layers), where the impact ionization process originates, is experimentally confirmed by the voltage contrast method.[63] The strong-field layer corresponds to the cathode dark space in a glow discharge. In the region $[\Delta+d,L]$ the potential varies slowly. In the glow discharge this region corresponds to the positive column. The coefficient of the electron current amplification γ is analogous to the coefficient of the secondary electron emission from a cathode.

6. IMR effect

The observed IMR effect can be explained by the developed theoretical model. Action of the applied magnetic field results in two effects: (1) the domain structure of the granular film changes and (2) spins of ferromagnetic particles and localized electrons at the interface are aligned along the field direction. This leads to the growth of the barrier height, reduces the barrier transparency, and decreases the electron concentration at the barrier region. Due to the feedback formed in the avalanche process, small variations in the barrier height and its transparency lead to great changes in the current.

Two ways of the spin-polarized current injected into the SC can be supposed (Fig. 13): (1) injected electrons surmount the spin-dependent potential barrier W at the distance r_0 from the interface and (2) spin-polarized electrons tunnel from sublevels of the exchange-splitted localized states. We consider the first way and neglect electron tunneling from localized states. The applied magnetic field reduces the transparency of the barrier. If the magnetic field H is less than the saturation field H_{sat} in which domains disappear, the domain structure of the granular film (Fig. 1) induces corresponding spin orientations of electrons localized in the accumulation layer in the SC and this induced domain structure has domain walls (Fig. 14). In this case, electrons injected from the granular film can cross through the accumulation layer without a loss of their spin polarization and without surmounting the potential barrier on channels close to domain walls (trajectories with points a). The average concentration of electrons, which trigger the avalanche process, is given by the sum of electron concentrations in regions with maximum height of the spin-dependent potential barrier (surface C in Fig. 14)

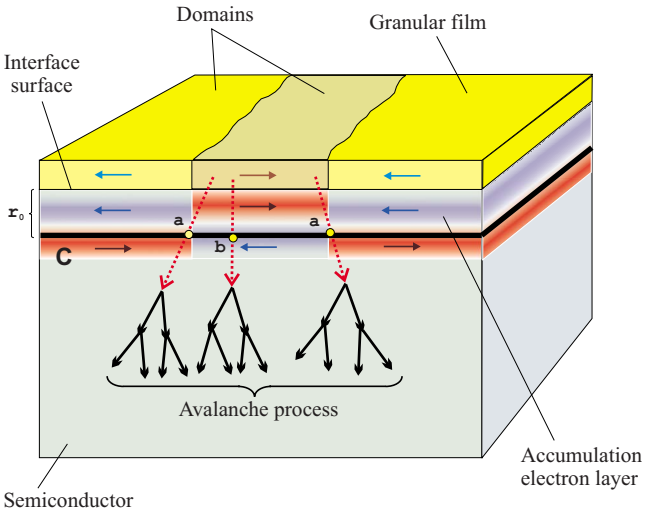

FIG. 14. (Color online) Trajectories without spin-flip scattering of injected electrons and without surmounting the potential barrier on the accumulation layer (points a) and trajectories with surmounting the potential barrier (points b). Surface C is the surface of maximum heights of the spin-dependent potential barrier.

$$n_C = n_a\xi_a + n_b\xi_b, \tag{24}$$

where n_a is the electron concentration in regions of domain walls, n_b is the electron concentration in domain regions, and ξ_a and ξ_b are contributions of partial concentrations to the average concentration. In the saturation magnetic field, $H=H_{sat}$, when domains disappear, electrons moving in the SC from the interface must surmount the potential barrier at the distance r_0 (trajectories with points b) and $\xi_a=0$ in Eq. (24). Taking into account that $n_a>n_b$ and the growth of the magnetic field reduces the contribution ξ_a of domain walls, from Eq. (24) one can find that in the range $[0,H_{sat}]$ increasing magnetic field leads to reduction in the electron concentration n_C.

At last, consider the barrier at the magnetic field $H>H_{sat}$. The applied magnetic field H presented in the Hamiltonian $\mathcal{H}_s$ interacts with spins $\vec{\sigma}(\vec{r})$ and $\vec{S}(\vec{r})$. For the magnetic field $H>H_{sat}$ there is alignment of spins of electrons in the accumulation layer and spins of ferromagnetic particles in the granular film with increasing magnetic field (Fig. 15). Magnetic field polarizes spins along the field direction. The field growth leads to the increase in the z-projection $\langle S_z(\vec{R})\rangle_0$, to the growth of the barrier height W [Eq. (9)], and to the reduction in the concentration n_b in Eq. (24). In this case, in the absence of domain walls, $\xi_a=0$ and $\xi_b=1$.

The avalanche process originates in the vicinity region of the barrier. The current density j flowing in the heterostructure is determined by the concentration of injected electrons n_C [Eq. (24)], the electron mobility μ_e, and the electrical field E_C at the surface C, $j=en_C\mu_eE_C$. Then, taking into account that $n_a=n_{int}\exp(eU_C/kT)$, $n_b=n_{int}\exp[(eU_C-W)/kT]$, where n_{int} is the electron concentration at the interface at the Fermi level, U_C is the difference of potentials between the interface and the surface C, from Eq. (1) for the tunnel opaque potential barrier we get

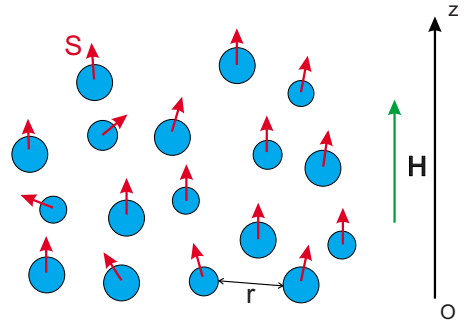

FIG. 15. (Color online) Alignment of spins of ferromagnetic particles at the interface of the SC/granular film heterostructure along the magnetic field direction. Distance r between ferromagnetic particles is a random parameter.

$$\mathrm{IMR}[W(H),T] = \frac{n_C(0)E_C(0)}{n_C(H)E_C(H)} - 1$$

$$= \frac{\{\xi_a(0)+\xi_b(0)\exp[-W(0)/kT]\}E_C(0)}{\{\xi_a(H)+\xi_b(H)\exp[-W(H)/kT]\}E_C(H)} - 1. \tag{25}$$

If $W(0)\gg kT$, for $H>H_{sat}$ contribution coefficients $\xi_a(H)=0$ and $\xi_b(H)=1$, and the magnetoresistance IMR [Eq. (25)] is rewritten in the simple form

$$\mathrm{IMR}[W(H),T] = A\exp\left[\frac{W(H)}{kT}\right] - 1, \tag{26}$$

where $A=\xi_a(0)E_C(0)/E_C(H)$. Taking into account that the energy barrier $W(H)$ sharply depends on temperature,[39] in the first approximation the temperature dependence of the IMR is determined by the term $\exp[W(H)/kT]$. The dependence of IMR on the applied electrical field is determined by the coefficient A. It depends on the ratio of the electrical field E_C at the surface C in the absence of a magnetic field and in the magnetic field H, respectively. When the avalanche process has been developed in the absence of a magnetic field, the voltage U_2 [Eq. (21)] is determined by the minimum value with $d=d_m$ [Eq. (23)], $U_2=E_dd_m$. Therefore, the electrical field $E_C(0)$ is high. When the magnetic field suppresses the onset of the impact ionization, distribution of the applied voltage $U=U_1+U_2$ (Fig. 13) changes. In the absence of the avalanche process the voltage U_2 is equal to a high value. This causes decreasing the voltage U_1 and decreasing the field $E_C(H)$ with respect to the field $E_C(0)$ without a magnetic field. The coefficient A leads to high values.

B. Explanation of the experiment

In order to explain high values of the IMR effect in SiO_2(Co)/GaAs heterostructures and the temperature-peak-type character, we use the developed theoretical model. The developed theory can be applied for these heterostructures, if the size of Co nanoparticles is less than the thickness l of the accumulation layer. In this case, the granular film can be considered as continuous and can be characterized by statistical-average parameters. The thickness l depends on the difference of the chemical potentials $\Delta\mu=\mu_g-\mu_s$, where

μ_s is the chemical potential in the SC and μ_g is the chemical potential in the granular film. In the first approximation, the chemical potential μ_g is given by

$$\mu_g = \mu_{SiO_2}(x_{SiO_2}/100) + \mu_{Co}(x_{Co}/100),$$

where μ_{SiO_2} and μ_{Co} are the chemical potentials of the SiO_2 matrix and Co nanoparticles; x_{SiO_2} and x_{Co} are the atomic concentrations of the SiO_2 and Co in percents, respectively. The difference $\Delta\mu$ between chemical potentials of the GaAs and the SiO_2(Co) granular film and between chemical potentials of the Si substrate and the granular film can be estimated from well-known values of the energy of the thermoelectron emission. For the given materials the differences of the chemical potentials are $\mu_{SiO_2}-\mu_{Co}=0.59$ eV, $\mu_{SiO_2}-\mu_{GaAs}=0.62$ eV, $\mu_{Co}-\mu_{GaAs}=0.03$ eV, $\mu_{SiO_2}-\mu_{Si}=0.95$ eV, and $\mu_{Co}-\mu_{Si}=0.36$ eV.[64]

In order to solve Eqs. (2), (3), and (7) in the approximation of the continuous granular film model, we need to find the surface probability of the Co particle distribution at the interface. We assume that at the interface Co particles are randomly allocated with the surface probability

$$s = \bar{p}^{2/3} = \left[\frac{x_{Co}v_{Co}}{x_{Co}v_{Co} + (100 - x_{Co})v_{SiO_2}}\right]^{2/3},$$

where $\bar{p}$ is the relative Co volume; $v_{Co}=m_{Co}/\varrho_{Co}N_A$ and $v_{SiO_2}=m_{SiO_2}/\varrho_{SiO_2}N_A$ are atomic and molecular volumes for the Co and the SiO_2 matrix; m_{Co} and m_{SiO_2} are the respective atomic and molecular masses; ϱ_{Co} and ϱ_{SiO_2} are the densities of Co particles and the SiO_2 matrix; N_A is the Avogadro number. For calculations we use $m_{Co}=58.93$ a.m., $m_{SiO_2}=60.09$ a.m., $\varrho_{Co}=8.90$ g/cm^3, $\varrho_{SiO_2}=2.26$ g/cm^3.[65] According to the continuous granular film approximation, we must made substitutions $\langle\vec{S}(\vec{R})\rangle_0 \rightarrow s\langle\vec{S}(\vec{R})\rangle_0$ and $\langle S_z(\vec{R})\rangle_0 \rightarrow s\langle S_z(\vec{R})\rangle_0$ in relations (6) and (9), respectively.

Using the developed model, we have found the electron wave function $\chi_\nu(x)$ [Eq. (2)], the inner self-consistent electrical field $\varphi(\vec{r})$ [Eq. (3)], and the energy barrier W [Eq. (9)]. Calculations have been made for the effective exchange interaction $J_0(\vec{r}-\vec{R})=J_0\exp(-\xi|\vec{r}-\vec{R}|)$ with $J_0=2$ eV and $\xi=2$ nm^{-1}.[59] For SiO_2(Co)/GaAs heterostructures at the given temperatures 160–340 °C the thickness l of the accumulation layer is in the range 8–50 nm. The size of Co nanoparticles is less than the thickness l and the approximation of the continuous granular film is truthful. Heterostructures possess localized electron states in the accumulation layer at the interface. In contrast, for SiO_2(Co)/Si heterostructures due to higher values of the difference of the chemical potentials $\Delta\mu$ at the interface the potential depth of the accumulation layer is deeper. This leads to higher electron concentration at the interface and to more efficient shielding of Co spins. As a result of this, the accumulation layer has small thickness without any localized states. The absence of localized states in SiO_2(Co)/Si heterostructures explains small values of the barrier W [Eq. (9)]. Small height of the barrier results in small variations in W, when the magnetic field is changed, and small values of the IMR effect (Figs. 6 and 7) in comparison with IMR values in SiO_2(Co)/GaAs heterostructures (Figs. 4, 5, 8, and 9). Let us consider IMR dependencies on the Co concentration, temperature, and the magnetic field.

1. IMR dependence on the Co concentration

The dependence of the IMR on the Co concentration x for SiO_2(Co)/GaAs structures, when electrons are injected from the SiO_2(Co) film (Fig. 5), demonstrates high IMR values for the concentration range $x=54-71$ at. % and low IMR values for lower and higher Co concentrations. From the developed model it is found that structures with $x=54-71$ at. % have one to two electron localized states with high energies $\varepsilon_\lambda^{(ex)}$ [Eq. (6)], which leads to high barrier W at room temperature. Heterostructures with lower Co concentration ($x<54$ at. %) possess greater number of localized states in the accumulation layer with energies $\varepsilon_\lambda^{(ex)}$ of small values. For these structures the barrier height is small and the IMR coefficient is low. If the Co concentration $x>71$ at. %, the accumulation layer has small thickness without localized states and is transparent for current. This leads to small IMR values, too.

2. Temperature dependencies of the IMR

At the interface the electron concentration increases with temperature increasing. At low temperatures the accumulation layer contains large number of exchange-splitted localized states with small energies $\varepsilon_\lambda^{(ex)}$. Temperature increasing induces thinning of the accumulation layer, a decrease in the localized state number, an increase in energies $\varepsilon_\lambda^{(ex)}$, and a growth of the barrier W. At a certain temperature the accumulation layer contains one exchange-splitted level and the magnitude of W reaches the maximum value. The further temperature growth gives higher electron concentration at the interface, more efficient shielding of Co spins, and thinner thickness of the accumulation layer. When the sublevel, on which electrons have spin orientations opposite to Co spins, crosses the Fermi level, the height of the potential barrier W sharply decreases. In Fig. 2 for the SiO_2(Co)/GaAs structure with the Co content 71 at. % crossing of the Fermi level is manifested as a fall on the temperature dependence of the inject current at $T=320$ K at the applied voltage $U=70$ V. This fall in the current corresponds to the disappearance of the IMR effect at 320 K, $U=70$ V in Fig. 8.

The temperature-peak-type character of the IMR effect is presented in Figs. 8 and 9. Maxima of peaks correspond to one exchange-splitted level in the accumulation layer. Neglecting spin-polarized tunneling from exchange-splitted localized states, we fit experimental results using the relation (26). The barrier W is given by Eq. (9) and the amplitude A in the relation (26) is determined to reach the best fit of the peak height. According to the developed model, the peak width is inversely proportional to the magnitude of the surface probability s of the Co particle distribution at the interface. Decreasing the Co content results in the decrease in the surface probability s: from $s=0.52$ ($x=71$ at. % Co) to $s=0.26$ ($x=38$ at. % Co). This corresponds to the observed increase in the peak width with Co concentration decreasing: from $\Delta T=37$ K ($x=71$ at. % Co) to $\Delta T=62$ K ($x=38$ at. % Co).

Locations of IMR temperature peaks can be shifted by the applied electrical field. These shifts can be explained by the change in the electron concentration at the interface under the electrical field action. The applied field causes to an electron depletion in the SC at the interface. As a result of this, at high-field magnitudes it needs higher temperatures to form the accumulation layer with one exchange-splitted level. In order to take into account the action of the electrical field for the SiO_2(Co)/GaAs structure with the Co content 71 at. % in Fig. 8, we use the following differences of the chemical potentials $\Delta\mu$:0.201 eV (U=40 V), 0.197 eV (U=50 V), 0.187 eV (U=60 and 70 V).

3. IMR dependencies on the magnetic field

At last, we consider IMR dependencies on the magnetic field for SiO_2(Co)/GaAs structures. As we can see from Fig. 4, at magnetic fields of low values the IMR grows greater than at high magnetic fields. The high growth of the IMR can be explained by changes in the domain structure, which disappears at H_{sat}=4 kOe. Slow IMR increasing at the magnetic field $H > H_{sat}$ can be due to alignment of different spin orientations of randomly allocated Co particles at the interface (Fig. 15). Magnetic field polarizes spins along the field direction. This leads to the increase in the z-projection $\langle S_z(\vec{R})\rangle_0$ and to the increase in the barrier height W [Eq. (9)] with growth of the magnetic field. Higher barrier height suppresses the onset of the avalanche process. This changes the potential distribution and decreases the electrical field $E_C(H)$ (Figs. 13 and 14) in comparison with the electrical field $E_C(0)$ in the absence of a magnetic field. As a result of this the value of the coefficient A in Eq. (26) becomes higher with magnetic field increasing.

IV. EXTENSION OF THE IMR EFFECT ON HETEROSTRUCTURES WITH OTHER SEMICONDUCTORS

We have considered SiO_2(Co)/GaAs heterostructures and have come to the conclusion that these heterostructures can be used as (1) spin-polarized electron injectors and (2) efficient magnetoresistive sensors. Spin-polarized electron injection can be observed at low voltages in the absence of an avalanche process. Electrons tunnel from exchange-splitted localized states in the accumulation layer (Fig. 13). If the tunneling transparency in the region $[\gamma_1, \gamma_2]$ from the highest sublevel is greater than the transparency from lower sublevels, then the spin injection reaches high values. Magnetoresistive sensors are based on the IMR effect in SiO_2(Co)/GaAs heterostructures, which is observed at high voltages above the threshold of the avalanche process. The developing impact ionization produces holes, which move and are accumulated in the region of the potential barrier. Formed positive feedback leads to great changes in the flowing current. But this process has some deficiencies. (1) The IMR effect in SiO_2(Co)/GaAs heterostructures has the temperature-peak-type character. (2) This effect is observed in heterostructures with semi-insulating GaAs and in heterostructures with n-GaAs of high resistivity.

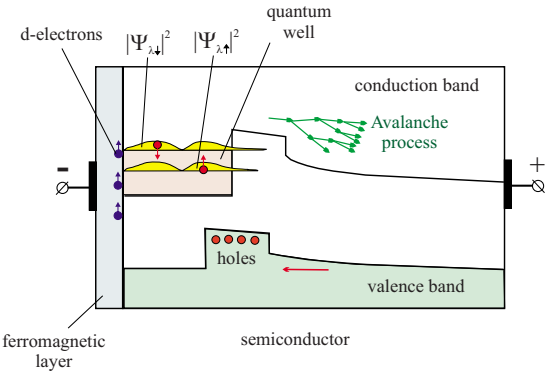

FIG. 16. (Color online) Schematic band diagram of the magnetoresistive sensor on the base of the heterostructure with quantum well and hole trap in the avalanche regime.

It is very important to extend the IMR effect observed in SiO_2(Co)/GaAs heterostructures to heterostructures with other SCs and to reach the IMR coefficient of high values in a broad temperature range. One of the promising semiconductor for spintronics with enhanced lifetime and transport length is silicon, Si.[19,46,66] Spin-orbit effects producing spin relaxation are much smaller in Si than in GaAs owing to the lower atomic mass and the inversion symmetry of the crystal structure maintaining spin-degenerate bands. Furthermore, the most abundant isotope ^{28}Si has no nuclear spin, suppressing hyperfine interactions. These properties make relatively long spin lifetimes in Si.

Considering the IMR effect in SiO_2(Co)/GaAs heterostructures, we can result in conclusion that for the efficient magnetoresistance in FM/SC heterostructures it is needed to fulfill the following requirements. (1) The SC contains a quantum well at the interface. (2) The quantum well must contain localized electron levels. (3) Localized levels must be exchange splitted by the FM. Interaction with electrons on these levels forms the spin-dependent barrier. (4) Giant magnetoresistance effect can be achieved in the presence of the impact ionization process. (5) The trap for holes produced by the impact ionization must be placed in the region of the potential barrier. Holes lower the barrier height. This forms the positive feedback and results in great changes in the current.

The studied SiO_2(Co)/GaAs heterostructures contain quantum wells formed by the SiO_2(Co) film due to the difference of the chemical potentials between the SiO_2(Co) and the GaAs. Width and form of these quantum wells are strongly dependent on the electron concentration at the interface and, therefore, on temperature. Using another methods to form quantum wells at interfaces in SCs (molecular-beam epitaxy and metal-organic chemical-vapor deposition), we can obtain quantum wells with desired width, depth, and number of localized electron levels. Magnetoresistive sensors with use the impact ionization process can be constructed on the base of heterostructures with hole traps and quantum wells near the interface (Fig. 16). Localized levels can be splitted by the exchange interaction with a FM grown at the interface or by the interaction with a granular film containing FM nanoparticles. It is needed to note that the latter technology method—sputtering of the granular film

can solve the problem of the efficient spin injection difficulty due to the inherent conductivity mismatch between FM metals and SCs.[67] Variation in the FM nanoparticle concentration leads to considerable variation in the conductivity of the granular film and we can reach conductivity correspondence between the FM and the SC. The additional barrier formed near the quantum well in the region of the hole trap makes possible to improve the onset of the impact ionization Applied voltage drops on the barrier and, thus, forms high electrical field in this region sufficient to start the avalanche process.

It can be expected that the proposed magnetoresistive sensor possesses the magnetoresistive effect of high values in a broad temperature range. The quantum well has fixed width and depth. This leads to a fixed number of localized levels, which are responsible for the formation of the spin-dependent barrier. The number of levels is slightly dependent on temperature. There is the reason to believe that the magnetoresistive sensor based on this heterostructure can operate at a broader temperature range in comparison with sensors based on SiO_2(Co)/GaAs heterostructures in which the quantum well at the interface is formed by the difference of chemical potentials of the GaAs and the granular film.

V. CONCLUSION

We have studied the electron-spin transport in SiO_2(Co)/GaAs and SiO_2(Co)/Si heterostructures, where the SiO_2(Co) structure is the granular SiO_2 film with Co nanoparticles and have obtained the following results.

(1) In SiO_2(Co)/GaAs heterostructures the giant IMR effect is observed. The IMR effect has positive values and the temperature-peak-type character. The temperature location of the effect depends on the Co concentration and can be shifted by the applied electrical field. For the SiO_2(Co)/GaAs heterostructure with 71 at. % Co the IMR value reaches 1000 (10^5%) at room temperature, which is two to three orders higher than maximum values of GMR in metal magnetic multilayers and TMR in magnetic tunnel junctions. On the contrary, for SiO_2(Co)/Si heterostructures magnetoresistance values are very small (4%) and for SiO_2(Co) films the intrinsic magnetoresistance is equal to opposite values.

(2) High values of the magnetoresistance effect in SiO_2(Co)/GaAs heterostructures have been explained by magnetic field-controlled onset of the impact ionization. The spin-dependent potential barrier is formed in the accumulation electron layer in the semiconductor near the interface. The impact ionization induced by injected electrons produces holes, which move and are accumulated in the region of the potential barrier. Existence of holes in the region of the barrier lowers the barrier height, grows the electron current flowing through the barrier, and leads to the enhancement of the avalanche process. Due to the formed positive feedback small variations in the barrier height give great changes in the current. The applied magnetic field increases the height and reduces the transparency of the barrier. This suppresses the onset of the impact ionization and changes the potential distribution. The developed model can explain some features of experimental results. The spin-dependent potential barrier is due to the exchange interaction between electrons in the accumulation electron layer in the SC and *d* electrons of Co. Existence of localized electron states in the accumulation layer results in high values and the temperature-peak-type character of the barrier in the SiO_2(Co)/GaAs. This leads to the temperature-peak-type character of the IMR. Maxima of IMR peaks correspond to one exchange-splitted level in the accumulation layer. The temperature peak width is inversely proportional to the surface probability of the Co particle distribution at the interface. In contrast, for SiO_2(Co)/Si heterostructures the accumulation layer has small thickness without any localized states, is tunnel transparent and does not influence on the injection current.

(3) FM/SC heterostructures with quantum wells containing spin-polarized localized electrons in the SC at the interface are proposed as efficient room-temperature spin injectors. In the avalanche regime heterostructures with holes traps and spin-dependent potential barrier in quantum wells can be used as efficient magnetic sensors.

ACKNOWLEDGMENTS

The authors gratefully acknowledge the assistance of V. M. Lebedev (PNPI, Gatchina, Leningrad region, Russia) for determination of the film composition, M. V. Baidakova (A.F. Ioffe Physico-Technical Institute, St. Petersburg, Russia) for the measurements by the small-angle x-ray scattering method, and S. Yu. Krasnoborod'ko (NT-MDT, Russia) for MFM images of the domain structure of samples. We would like to thank Yu. G. Kusrayev, V. I. Kozub, and V. L. Korenev for useful discussions. This work was supported by the Russian Foundation for Basic Research under Grant No. 10-02-00516.

*l_lutsev@mail.ru

[1] S. A. Wolf, D. D. Awschalom, R. A. Buhrman, J. M. Daughton, S. von Molnar, M. L. Roukes, A. Y. Chtchelkanova, and D. M. Treger, Science **294**, 1488 (2001).
[2] G. Schmidt, J. Phys. D **38**, R107 (2005).
[3] I. Žutic, J. Fabian, and S. Das Sarma, Rev. Mod. Phys. **76**, 323 (2004).
[4] B. P. Zakharchenya and V. L. Korenev, Phys. Usp. **48**, 603 (2005).
[5] R. Bertacco, M. Riva, M. Cantoni, F. Ciccacci, M. Portalupi, A. Brambilla, L. Duo, P. Vavassori, F. Gustavsson, J.-M. George, M. Marangolo, M. Eddrief, and V. H. Etgens, Phys. Rev. B **69**, 054421 (2004).
[6] G. Schmidt, G. Richter, P. Grabs, C. Gould, D. Ferrand, and L. W. Molenkamp, Phys. Rev. Lett. **87**, 227203 (2001).
[7] Y. Ohno, D. K. Yong, B. Beschoten, F. Matsukura, F. Ohno, and D. D. Awschalom, Nature (London) **402**, 790 (1999).
[8] B. T. Jonker, Y. D. Park, B. R. Bennett, H. D. Cheong, G. Ki-

‘oseoglou, and A. Petrou, Phys. Rev. B **62**, 8180 (2000).
[9] A. Hirohata, Y. B. Xu, C. M. Guertler, and J. A. C. Bland, J. Appl. Phys. **87**, 4670 (2000).
[10] A. Hirohata, Y. B. Xu, C. M. Guertler, J. A. C. Bland, and S. N. Holmes, Phys. Rev. B **63**, 104425 (2001).
[11] A. F. Isakovic, D. M. Carr, J. Strand, B. D. Schultz, C. J. Palmstrøm, and P. A. Crowell, Phys. Rev. B **64**, 161304(R) (2001).
[12] Z. H. Xiong, D. Wu, Z. V. Vardeny, and J. Shi, Nature (London) **427**, 821 (2004).
[13] A. T. Hanbicki, B. T. Jonker, G. Istkos, G. Kioseoglou, and A. Petrou, Appl. Phys. Lett. **80**, 1240 (2002).
[14] H. J. Zhu, M. Ramsteiner, H. Kostial, M. Wassermeier, H.-P. Schönherr, and K. H. Ploog, Phys. Rev. Lett. **87**, 016601 (2001).
[15] P. R. Hammar, B. R. Bennett, M. J. Yang, and M. Johnson, Phys. Rev. Lett. **83**, 203 (1999).
[16] P. R. Hammar and M. Johnson, Appl. Phys. Lett. **79**, 2591 (2001).
[17] X. Jiang, R. Wang, R. M. Shelby, R. M. Macfarlane, S. R. Bank, J. S. Harris, and S. S. P. Parkin, Phys. Rev. Lett. **94**, 056601 (2005).
[18] R. Mattana, J.-M. George, H. Jaffres, F. N. van Dau, A. Fert, B. Lepine, A. Guivarch, and G. Jezequel, Phys. Rev. Lett. **90**, 166601 (2003).
[19] B. T. Jonker, G. Kioseoglou, A. T. Hanbicki, C. H. Li, and P. E. Thompson, Nat. Phys. **3**, 542 (2007).
[20] M. N. Baibich, J. M. Broto, A. Fert, F. Nguyen Van Dau, F. Petroff, P. Etienne, G. Creuzet, A. Friederich, and J. Chazelas, Phys. Rev. Lett. **61**, 2472 (1988).
[21] G. Binasch, P. Grunberg, F. Saurenbach, and W. Zinn, Phys. Rev. B **39**, 4828 (1989).
[22] J. Bass and W. P. Pratt, Jr., J. Magn. Magn. Mater. **200**, 274 (1999).
[23] M. A. M. Gijs and G. E. W. Bauer, Adv. Phys. **46**, 285 (1997).
[24] J. S. Moodera, L. R. Kinder, T. M. Wong, and R. Meservey, Phys. Rev. Lett. **74**, 3273 (1995).
[25] J. S. Moodera and G. Mathon, J. Magn. Magn. Mater. **200**, 248 (1999).
[26] Xiu-Feng Han, M. Oogane, H. Kubota, Y. Ando, and T. Miyazaki, Appl. Phys. Lett. **77**, 283 (2000).
[27] E. Y. Tsymbal, O. N. Mryasov, and P. R. LeClair, J. Phys.: Condens. Matter **15**, R109 (2003).
[28] J. M. De Teresa, A. Barthelemy, A. Fert, J. P. Contour, F. Montaigne, and P. Seneor, Science **286**, 507 (1999).
[29] S. S. P. Parkin, C. Kaiser, A. Panchula, P. M. Rice, B. Hughes, M. Samant, and S.-H. Yang, Nature Mater. **3**, 862 (2004).
[30] S. Yuasa, T. Nagahama, A. Fukushima, Y. Suzuki, and K. Ando, Nature Mater. **3**, 868 (2004).
[31] S. Yuasa, A. Fukushima, H. Kubota, Y. Suzuki, and K. Ando, Appl. Phys. Lett. **89**, 042505 (2006).
[32] C. Tiusan, F. Greullet, M. Hehn, F. Montaigne, S. Andrieu, and A. Schuhl, J. Phys.: Condens. Matter **19**, 165201 (2007).
[33] Y. M. Lee, J. Hayakawa, S. Ikeda, F. Matsukura, and H. Ohno, Appl. Phys. Lett. **90**, 212507 (2007).
[34] V. A. Samuilov, V. K. Ksenevich, G. Remenyi, G. Kiss, and B. Pödör, Semicond. Sci. Technol. **14**, 1084 (1999).
[35] H. Akinaga, M. Mizuguchi, K. Ono, and M. Oshima, Appl. Phys. Lett. **76**, 357 (2000).
[36] Z. G. Sun, M. Mizuguchi, T. Manago, and H. Akinaga, Appl. Phys. Lett. **85**, 5643 (2004).
[37] L. V. Lutsev, A. I. Stognij, and N. N. Novitskii, JETP Lett. **81**, 514 (2005).
[38] L. V. Lutsev, A. I. Stognij, N. N. Novitskii, and A. A. Stashkevich, J. Magn. Magn. Mater. **300**, e12 (2006).
[39] L. V. Lutsev, J. Phys.: Condens. Matter **18**, 5881 (2006).
[40] M. Yokoyama, T. Ogawa, A. M. Nazmul, and M. Tanaka, J. Appl. Phys. **99**, 08D502 (2006).
[41] J. J. H. M. Schoonus, F. L. Bloom, W. Wagemans, H. J. M. Swagten, and B. Koopmans, Phys. Rev. Lett. **100**, 127202 (2008).
[42] J. J. H. M. Schoonus, J. T. Kohlhepp, H. J. M. Swagten, and B. Koopmans J. Appl. Phys. **103**, 07F309 (2008).
[43] J. Nordling, R. L. Millen, H. A. Bullen, M. D. Porter, M. Tondra, and M. C. Granger, Anal. Chem. **80**, 7930 (2008).
[44] R. L. Millen, J. Nordling, H. A. Bullen, M. D. Porter, M. Tondra, and M. C. Granger, Anal. Chem. **80**, 7940 (2008).
[45] I. Appelbaum, K. J. Russel, D. J. Monsma, V. Narayanamurti, C. M. Marcus, M. P. Hanson, and A. C. Gossard, Appl. Phys. Lett. **83**, 4571 (2003).
[46] I. Appelbaum and D. J. Monsma, Appl. Phys. Lett. **90**, 262501 (2007).
[47] K. J. Russell, I. Appelbaum, Wei Yi, D. J. Monsma, F. Capasso, C. M. Marcus, V. Narayanamurti, M. P. Hanson, and A. C. Gossard, Appl. Phys. Lett. **85**, 4502 (2004).
[48] A. I. Stognij, N. N. Novitskii, and O. M. Stukalov, Tech. Phys. Lett. **28**, 17 (2002).
[49] A. I. Stognij, N. N. Novitskii, and O. M. Stukalov, Tech. Phys. Lett. **29**, 43 (2003).
[50] T. K. Zvonareva, V. M. Lebedev, T. A. Polanskaya, L. V. Sharonova, and V. I. Ivanov-Omskii, Semiconductors **34**, 1094 (2000).
[51] S. Barzilai, Y. Goldstein, I. Balberg, and J. S. Helman, Phys. Rev. B **23**, 1809 (1981).
[52] K. Yakushiji, S. Mitani, K. Takanashi, J.-G. Ha, and H. Fujimori, J. Magn. Magn. Mater. **212**, 75 (2000).
[53] S. Sankar, D. Dender, J. A. Borchers, D. J. Smith, R. W. Erwin, S. R. Kline, and A. E. Berkowitz, J. Magn. Magn. Mater. **221**, 1 (2000).
[54] Yu. A. Izyumov, F. A. Kassan-ogly, and Yu. N. Skryabin, *Field Methods in the Theory of Ferromagnetism* (Nauka, Moscow, 1974).
[55] A. A. Abrikosov, L. P. Gor’kov, and I. E. Dzyaloshinski, *Methods of Quantum Field Theory in Statistical Physics* (Dover, New York, 1975).
[56] M. A. Ruderman and C. Kittel, Phys. Rev. **96**, 99 (1954).
[57] T. Kasuya, Prog. Theor. Phys. **16**, 45 (1956).
[58] K. Yosida, Phys. Rev. **106**, 893 (1957).
[59] W. A. Harrison, *Electronic Structure and the Properties of Solids. The Physics of the Chemical Bond* (Freeman, San Francisco, 1980).
[60] Yu. P. Raizer, *Gas Discharge Physics* (Springer-Verlag, Berlin, 1991).
[61] B. Chapman, *Glow Discharge Processes* (Wiley, New York, 1980).
[62] A. S. Kyuregyan and S. N. Yurkov, Sov. Phys. Semicond. **23**, 1126 (1989).
[63] J. J. Mareš, J. Krištofik, P. Hubik, K. Jurek, S. Pospišil, and J. Kubašta, J. Appl. Phys. **82**, 3358 (1997).
[64] V. S. Fomenko and I. A. Podchernyaeva, *Emission and Adsorp-*

tion Properties of Substances and Materials (Nauka, Moscow, 1975).

[65] *Handbook of Physical Quantities*, edited by I. S. Grigoriev and E. Z. Meilikhov (CRC, Boca Raton, 1997).

[66] I. Appelbaum, B. Huang, and D. J. Monsma, Nature (London) **447**, 295 (2007).

[67] G. Schmidt, D. Ferrand, L. W. Molenkamp, A. T. Filip, and B. J. van Wees, Phys. Rev. B **62**, R4790 (2000).